ISPRS Journal of Photogrammetry and Remote Sensing 234 (2026) 261–274

Contents lists available at ScienceDirect

ISPRS Journal of Photogrammetry and Remote Sensing

journal homepage: www.elsevier.com/locate/isprsjprs

Automatic tree-level based forest inventories retrieval via ultra-high resolution UAV images and deep learning

Wen Fan [a], Thomas Knoke [a], Jonas Troles [b], Jiaojiao Tian [a,c,*]

[a] Institute of Forest Management, TUM School of Life Sciences Weihenstephan, Technical University of Munich, 85354 Freising, Germany
[b] Cognitive Systems Group, University of Bamberg, 96047 Bamberg, Germany
[c] Remote Sensing Technology Institute (IMF), German Aerospace Center (DLR), 82234 Wessling, Germany

ARTICLE INFO

Keywords:
Individual tree crown
Tree species classification
Vitality estimation
Carbon stock estimation
Forest inventory
Deep learning

ABSTRACT

Forest inventories play an essential role in managing and protecting forest resources as well as quantifying carbon stocks. Recent advances in Uncrewed Aerial Vehicles (UAVs) have enhanced capabilities for efficiently monitoring forest dynamics across large geographic areas. RGB cameras are typically preferred for rapid and scalable forest inventory missions owing to three distinct advantages, including low cost, ease of use, and high resolution. However, compared with multispectral or hyperspectral sensors, the limited spectral signals of RGB cameras pose challenges for tree crown detection and classification. The ability of deep learning methods to capture structural and contextual cues from imagery helps alleviate some of the limitations of RGB data. In this study, we propose an Individual Tree Crown (ITC)-based framework leveraging UAV data and advanced deep learning models for inventories of individual trees in dense and natural forests. First, we develop the ITC-based Multi-Task Convolutional Neural Network (ITCMNet), which incorporates multi-scale contexts to simultaneously and accurately identify individual tree crowns, discriminate tree species, and assess tree vitality. Second, structural parameters for each individual crown are extracted to estimate forest carbon storage using species-specific allometric models. Unlike conventional pixel-based methods, our proposed ITCMNet enables precise forest investigations at the ITC level, enhancing both performance and interpretability. We collected a comprehensive dataset consisting of 2456 ultra-high resolution (1.6 cm) UAV RGB images and 27,160 labeled trees across 105 plots distributed in three dense forests and one city park in Germany to evaluate our framework. The ITCMNet demonstrated robust tree crown delineation performance, achieving an *F1 score* of 0.81. Additionally, our method attained an *F1 score* in species classification (i.e., 0.54 for angiosperms and 0.76 for gymnosperms) and vitality identification (0.66). Utilizing precise tree parameters, species information, and species-specific allometric models, our carbon storage estimation surpassed current satellite-based carbon products. The carbon stock estimation achieved an R^2 of 0.83 and the carbon storage range in the Bamberg forests is approximately 50 to 110 Mg C/ha. These results show that our proposed framework provides detailed, cost-effective forest inventories, highlighting its potential to support various downstream forestry applications. The dataset and source code are available (https://www.dlr.de/en/eoc/about-us/remote-sensing-technology-institute/photogrammetry-and-image-analysis/public-datasets/bamforests; https://github.com/WendyFan52/ITCMNet).

1. Introduction

Approximately one-third of Germany's forest is under unprecedented stress (Riedel et al., 2024). Between 2018 and 2021, satellite data revealed that around 501,000 ha of forest in Germany experienced severe canopy loss, accounting for approximately 5% of the country's total forest area (Knutzen et al., 2025). Timely forest inventory data is essential for the prompt implementation of intervention measures. Forest inventories with intense field work to monitor forest dynamics at a large scale are expensive and laborious (Liang et al., 2022). For the Fourth National Forest Inventory of Germany, around 100 specially trained survey teams from the federal states measured around 521,000 trees in 2021 and 2022, and the data quality assessment took two years until 2024 (Riedel et al., 2024). However, the information provided by

* Corresponding author.
E-mail addresses: wendy.fan@tum.de (W. Fan), knoke@tum.de (T. Knoke), jonas.troles@uni-bamberg.de (J. Troles), Jiaojiao.Tian@dlr.de (J. Tian).

https://doi.org/10.1016/j.isprsjprs.2026.02.029
Received 8 July 2025; Received in revised form 19 February 2026; Accepted 19 February 2026

inventories is indispensable for making informed management decisions. Monitoring the change in forest composition and configuration is important to facilitate the forest's adaptation to climate change and to assess the provisioning of ecosystem services and the sustainability of past forest management (Hahn and Knoke 2010). Moreover, quantifying forest carbon storage services is fundamental for estimating forests' environmental and economic value and supporting their conservation (Knoke et al., 2023). Since 2017, Germany's forests have lost 41.5 million tonnes of carbon, highlighting the urgent need for adaptation and restoration measures (Riedel et al., 2024). Compared to traditional fieldwork, combined field surveys and remote sensing can be more cost-effective and efficient for large-scale forest inventory missions (Lechner et al., 2020). However, its low spatial resolution from satellite sensors (10 m −1 km) can lead to a mismatch between remote sensing pixels and individual trees. One pixel contains information from multiple tree crowns (Ferrara et al., 2023). Although LiDAR provides information at the level of individual trees, the high cost of data acquisition and processing makes it impractical for large-scale applications (Yao et al., 2021).

Advances in UAVs enable the acquisition of high-resolution imagery at lower costs and with easy processing, allowing individual tree crown detection to be matched with field forest inventory records (Puliti et al., 2017; Wallace et al., 2012). Recently, UAVs with advanced sensors (e.g., multispectral, hyperspectral, or LiDAR) have been widely used for the extraction of critical forest parameters, including tree height, canopy cover, crown delineation, and species identification through photogrammetry and machine learning techniques (Hu et al., 2020; Weinstein et al., 2021a). Compared to other sensors, RGB cameras offer rapid data acquisition at significantly lower operational costs and require less complex post-processing procedures, which is particularly advantageous for forest inventories over large geographical areas. However, owing to their limited spectral bands and lack of structural information, RGB cameras face challenges in accurately distinguishing subtle vegetation characteristics, detecting stress indicators, modeling complex forest structures, as well as quantifying forest carbon storage (Diez et al., 2021; Qin et al., 2022; Schiefer et al., 2020). These limitations highlight the need for developing advanced methods and innovative workflows to enhance the extraction of precise and reliable forest inventory information from RGB imagery alone.

Rich spatial contexts in high-resolution imagery offer a solution to mitigate the limited spectral information from RGB imagery. The spatial extent of individual trees allows spatial information to be aggregated more effectively for analyzing tree status. ITC delineation using high-resolution UAV imagery is a widely adopted method that facilitates the identification of unique tree characteristics and additional attributes, such as crown size, area, and spatial location (Jing et al., 2012; Wagner et al., 2018). One of the classical ITC approaches is the Watershed Algorithm (Tochon et al., 2015), which searches for local point maxima in the image to be used as seed points for region growing and segmentation based on a high-resolution canopy height model (CHM) derived from UAV images or LiDAR (Kempf et al., 2021; Liu et al., 2024). Although this method is widely used for many applications due to its simplicity, its performance is still limited because seed points may be incorrectly detected due to inaccurate CHM in areas of varying tree density (Wen et al., 2024). As for classification tasks, machine learning algorithms, such as random forest and support vector machine, are usually used for pixel-based tree species classification (Feng et al., 2015; Hartling et al., 2021). However, when only UAV RGB data is available, these pixel-based algorithms are limited to capturing subtle differences due to their fewer spectral signals and because they ignore abundant textures from high-resolution imagery.

Fortunately, advanced deep learning methods have demonstrated superiority over other approaches in detecting tree objects, owing to their strong ability to capture spatiotemporal context from remote sensing observations (Wen et al., 2024; Zheng et al., 2021). Convolutional Neural Networks (CNNs) are a powerful category of deep learning models specifically designed for processing and analyzing image data by automatically learning hierarchical spatial features directly from raw pixels (Li et al., 2021a; Liu et al., 2022a). Regarding forest inventories using UAV RGB data, CNNs also demonstrated superior performance in capturing local features and handling high-resolution images for tree detection and classification (Brandt et al., 2024; Schiefer et al., 2020). Early studies mainly focused on pixel-level single tasks, such as tree segmentation or classification, using UAV or high-resolution satellite imagery for forest monitoring (Liang et al., 2025; Xu et al., 2021). More recently, instance-level ITC segmentation and classification methods have been developed by using UAV RGB imagery, allowing for the extraction of more detailed structural information at the level of individual trees. Although RGB imagery provides valuable information for tree species, its effectiveness is often limited by factors such as class imbalance, ambiguous boundaries, and spectral similarity among species, which constrain classification accuracy (Ecke et al., 2024). As summarized in Table 1, many existing forest research studies focus on a single task, while there has been increased in attention paid to the joint task of tree species classification and ITC segmentation, in order to explore the potential of ultra-high resolution RGB imagery for mapping mixed forests (Schiefer et al., 2020). Modeling these tasks jointly can further improve performance. Low-cost forest inventory frameworks based on high-resolution imagery have been further explored. The potential of sub-meter aerial imagery for tree counting, canopy segmentation, and height prediction at a national scale has been demonstrated (Li et al., 2023). Furthermore, the performance of various UAV-based image sensors in ITC detection and species classification has been investigated. Compared to multispectral and hyperspectral data, RGB imagery offers the optimal cost-effectiveness, as its high spatial resolution facilitates superior tree detection and structural analysis (Nevalainen et al., 2025). In this study, we propose a multi-task framework at the instance level that performs individual tree detection, species classification, and vitality assessment simultaneously. Through the utilization or exploitation of shared features among these tasks, the framework improves overall performance.

To address the challenges mentioned above, this paper presents a framework to deal with individual tree-level attribute inventories. The objective is to predict the location, species, vitality, aboveground biomass (AGB), and carbon stocks of individual trees. ConvNeXt combines the strengths of CNNs with a transformer-inspired structure (Liu et al., 2022b). Specifically, we developed the ITC-based Multi-Task Convolutional Neural Network (ITCMNet) using ConvNeXt V2 as the modern backbone. Moreover, the proposed ITCMNet is designed to deal with both segmentation and classification tasks together, so that the classification tasks, including species classification and vitality identification, can be improved by utilizing textures from different ITCs. Following this, the ITC-level forest carbon storage is estimated using structural parameters from delineated crown shapes, CHM, and species-specific allometric models. To evaluate the proposed framework, we collected a total of 2456 ultra-high resolution UAV images and 27,160 annotated trees (i.e., crown boundary, species, and vitality) in four forests in Germany. To demonstrate the capability of the proposed method, we also compare it with the Swin Transformer, U-Net, and satellite-based datasets for segmentation, classification, carbon estimation tasks.

2. Study area and data

2.1. Study region

The study area is located near Bamberg, Bavaria, Germany. The climate of Bamberg is classified as marine west coast with some continental influence, and there is significant rainfall throughout the year. The average annual temperature in the region is 10.34°C. Data were collected from forests and urban parks within a 20-kilometer radius around Bamberg (Troles et al., 2024). The Bamberg region consists of

Table 1
Comparison of methods for individual tree segmentation and classification.

Category	Representative Methods	Strengths	Limitations
CHM-based tree segmentation	Watershed algorithm	Simple, efficient, and widely used in forestry.	Sensitive to CHM quality; fails in dense/ overlapping canopies.
Machine learning for tree classification	Random Forest, SVM	Robust with limited data, interpretable and fast.	Relies on manual features, weak spatial context in RGB imagery.
Single-task deep learning	CNN, Transformer, or Mamba-based segmentation or classification models	State-of-the-art accuracy, automated spatial feature extraction	Single-objective focus, large annotated datasets
Multi-task deep learning	Joint CNN, Transformer, or Mamba-based frameworks	Shared feature representation, efficient and highly consistent.	Under-researched for RGB-only UAVs, high architectural complexity

data from four different Areas of Interest (AOIs). A total of 105 sample plots has been annotated for the BAMFORESTS dataset (shown in Fig. 1). In Fig. 1, each red dot represents a single sample plot. Each sample plot covers one hectare. Described by (Troles et al., 2024), the Hain AOI is an urban forest park of approximately 61 ha. The Stadtwald AOI covers 152 ha and is located about 5 km southeast of Bamberg city center. The Tretzendorf-1 AOI covers 65 ha, while the Tretzendorf-2 AOI covers 47 ha. Of the annotated tree areas, the sample plot area from the Hain AOI covers 15 ha. The sample plot area in the Stadtwald AOI covers 46 ha and the sample plot area in the Tretzendorf AOI consists of two regions, one covering 29 ha and the other 15 ha, respectively, as shown in Fig. 1. The study area shows a rich diversity of tree species (given average German conditions), with seven prevailing species. Specifically, the main tree species are *Scots pine*, *European beech, Oak, Norway spruce, European larch, Douglas fir*, and *silver fir*. In terms of spermatophyte classification, *European beech* and *oak* are angiosperms, while the other five species are gymnosperms. This classification plays an important role in estimating AGB and carbon storage.

2.2. Benchmark data

This study primarily utilized the BAMFORESTS dataset along with the corresponding Digital Surface Model (DSM) (Troles et al., 2024) and public Digital Terrain Model (DTM) (Vermessungsverwaltung 2022) for the study area. The DSM was generated from multi-view UAV imagery using Structure from Motion (SfM) and stereo matching algorithms implemented in Agisoft Metashape (Agisoft, 2021). The DTM was obtained from publicly available airborne LiDAR data with a spatial resolution of 1 m and full coverage of the Bavarian region, provided by the Bavarian State Government (Vermessungsverwaltung 2022). To evaluate the accuracy of the DTM, random ground points without vegetation cover were selected for validation. The evaluation indicated that the DTM error is within ± 40 cm. BAMFORESTS contains 27,160 labeled trees of the 105 sample plots. A COCO format dataset with a resolution of 2048 × 2048 pixels is used (Lin et al., 2014). The images have a 50% overlap in both horizontal and vertical directions. The images are captured with two RGB sensors with slightly different resolutions and fields of view to collect data in Bamberg (Troles et al., 2024). The 20 MP, 1″ CMOS sensor provides a wider coverage suitable for urban areas with an 84°angle of view (AOV), while the 42.4 MP Sony RX1 RII offers higher spatial resolution for capturing fine-scale canopy structures in forests with a 63°AOV. The UAV RGB images and overlapping images were collected in July 2022. RGB orthophotos, DSM and DTM have pixel resolutions of 1.6 cm or 1.8 cm, 3.2 cm or 3.6 cm, and 1 m, respectively. Based on the collected DSM and DTM images, further pre-processing was performed to obtain this area's CHM image.

The four regions within the study area show significant differences in tree species and density. Experienced foresters were responsible for annotating the data. Tree annotations represent the foresters' delineation of tree crown boundaries in the drone imagery, as well as their identification of tree species and classification of vitality. In addition to classifying the seven tree species mentioned above, 'other' categories

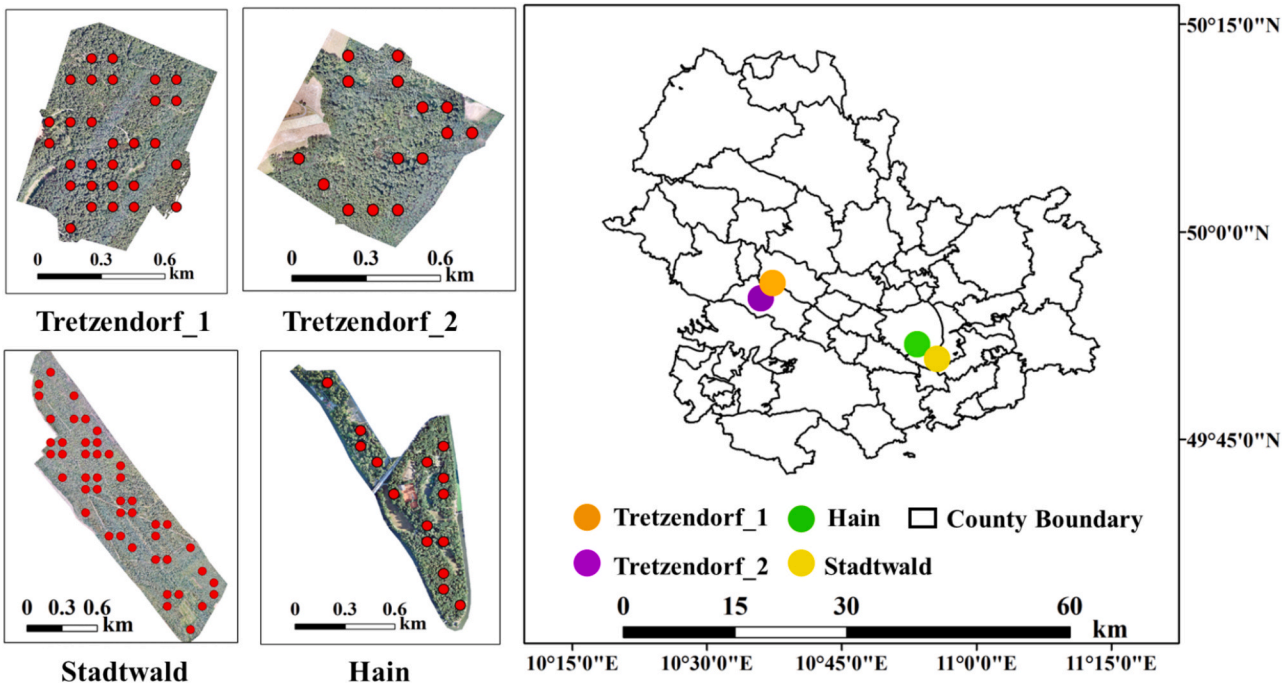

Fig. 1. The location of study areas and their surroundings in Bamberg, Germany.

were introduced for the species classification task. This ensures the ability of the model to generalize in complex forest environments. In the tree vitality estimation task, the number of classes is set to three, representing healthy, declining and dead trees. Healthy trees are easy to distinguish from dead trees. A declining tree has many dead branches, but it is not yet dead. Table 2 provides detailed information on individual tree annotations within the dataset, which are considered to represent the ground truth of individual trees in this study.

The *Train-set* refers to the dataset used to train the model, while the *Val-set* is used to evaluate the performance of the model during training, and the *Test-set* is used to evaluate the final performance of the model. The *Train-set* sample plots cover a total of 60 ha of forest, with 31 ha from the Stadtwald AOI and 29 ha from the Tretzendorf AOI. The *Val-set* sample plots cover 16 ha, with 8 ha from the Stadtwald AOI and 8 ha from the Tretzendorf AOI. The *Test-set* sample plots cover 29 ha in total, including 7 ha from Stadtwald AOI, 7 ha from Tretzendorf AOI, and 15 ha from Hain AOI. The Hain AOI sample plots are used exclusively for out-of-sample evaluation in the *Test-set*, which is not included in the *Train-set* or *Val-set*. The design of these plots plays a crucial role in the segmentation, classification, and evaluation of model performance.

In AGB and carbon stock estimation tasks, the ground truth is obtained by combining individual tree parameters with allometric equations. The tree parameters extracted by the proposed method are compared and evaluated with the ground truth.

3. Method

The proposed methodology in this study includes the two major steps: (1) Segmentation, classification and vitality estimation of individual trees in response to the needs of the forest inventory; (2) Carbon stock estimation using parameters from individual tree segmentation along with species-specific allometric models. The flowchart illustrates the data sources, methods, and sub-tasks of forest inventory in this paper (Fig. 2).

3.1. Multi-task learning

3.1.1. ITCMNet for tree segmentation and classification

In this study, a Multi-task Learning (MTL) strategy is employed to facilitate information sharing and mutual enhancement between individual tree instance segmentation and classification tasks (species classification and vitality classification) as shown in Fig. 2. Shared modules, such as the advanced Backbone and the Feature Pyramid Network (FPN), extract shared features across tasks. The extracted segmentation features and spatial information provide more accurate candidate regions for the Region Proposal Network (RPN), thereby improving the ability of the classification task to identify tree categories within these regions.

The design of ITCMNet is inspired by the framework of Mask R-CNN and ConvNeXt V2 (He et al., 2017; Woo et al., 2023). Due to its mature architecture and robustness in object detection and instance segmentation, Mask R-CNN has become a classic multi-task learning framework. The ConvNeXt represents a series of convolutional neural networks, with ConvNeXt V2 being an enhanced version of ConvNeXt. Its design is inspired by Vision Transformers, while retaining the efficiency and spatial properties of CNNs. Compared to the original ConvNeXt, its enhancements include utilizing a pre-trained Fully Convolutional Masked Autoencoder (FCMAE) for self-supervised learning and incorporating the Global Response Normalization (GRN) to enhance feature representation and diversity. Additionally, ConvNeXt V2 eliminates layer scale, reducing feature collapse issues and improving model stability on large-scale remote sensing imagery.

The output feature maps from different layers of the backbone ConvNeXt V2 are used to construct the FPN. By connecting these multi-level feature maps, the FPN performs multi-scale feature fusion. The high-level features contribute global contextual information, while low-level features preserve fine structural details. In tree crown detection, this design enables the model to effectively handle crowns of varying sizes. Then, the Region Proposal Network (RPN) module consists of AnchorGenerator and RPNHead. The AnchorGenerator provides prior anchors of different scales to accommodate varying tree crown sizes. The RPNHead generates potential candidate bounding boxes (BBox) for the tree crown based on prior anchors and performs the localization of the tree crown. Once candidate regions are proposed, the Region of Interest (RoI) Head, which consists of the BBox Head and the Mask Head, processes these regions in greater detail. The BBox Head consists of a two-layer Fully Connected (FC) network that provides output for object classification and regression, which is responsible for the regression of the BBox and precisely localizes the position of each tree crown. Based on the FCNMaskHead module, the Mask Head uses a four-layer convolutional structure to output the segmentation masks and generates a binary mask for each candidate region, allowing for segmentation of the tree crown area. Finally, to ensure optimal performance of the model, the total loss function consists of a weighted sum of the classification loss, the BBox regression loss and the mask loss. Classification loss is calculated using CrossEntropyLoss, which determines the category of each detected object. BBox regression loss is computed using L1Loss, which adjusts the predicted BBox to match the ground truth. Mask loss is calculated using CrossEntropyLoss, which measures the difference between the predicted segmentation mask and the ground truth mask. Through the integration of these loss functions, the model effectively optimizes both detection accuracy and segmentation precision, ensuring high-quality instance segmentation of trees.

3.1.2. Experimental parameter design

The dataset was divided into *Train-set, Test-set,* and *Val-set*. An epoch refers to one complete pass through the entire *Train-set*. Since datasets are often too large to process all at once, they are divided into smaller batches. In each training step, the model processes one batch of data, performs a forward pass, computes the loss, and updates the model parameters via backpropagation. During the training process, the number of epochs is 50, and the number of steps per epoch is determined by the size of the training dataset and a batch size of 2. At the beginning of each epoch, data is sampled sequentially from the shuffled dataset according to the batch size. During the epoch, all batches are iterated sequentially until the entire dataset has been accessed once. A learning rate warm-up phase is used for the first 1,000 steps, starting at 0.001 times the base learning rate. After reaching predefined milestones at epoch 40 and epoch 45, the learning rate is progressively reduced by a factor of 0.1 at each milestone. The learning rate decay is intended to improve convergence and avoid overfitting and oscillations. Model performance was evaluated on the validation set after each epoch. During training, the checkpoint hook automatically saved the model weights corresponding to the best validation performance and retained only the most recent checkpoint to save storage space while ensuring that the best model was available for evaluation. Loss values and evaluation metrics were continuously logged using the LoggerHook, enabling visualization of training and validation loss curves for monitoring convergence and stability. The model that performed best on the *Val-set* was used for all subsequent testing and analysis. Model robustness was further evaluated on the held-out test set using evaluation metrics, including BBox and mask performance. To gain deeper insight into class-level segmentation performance, the average precision (AP) for each class needs to be reported and compared.

The ITCMNet was implemented using MMDetection 3.0 (Chen et al.,

Table 2
BAMFORESTS 2048 × 2048 dataset.

	Train-set	Val-set	Test-set
Number of Images	1,439	382	635
Number of Annotations	58,235	15,180	19,041

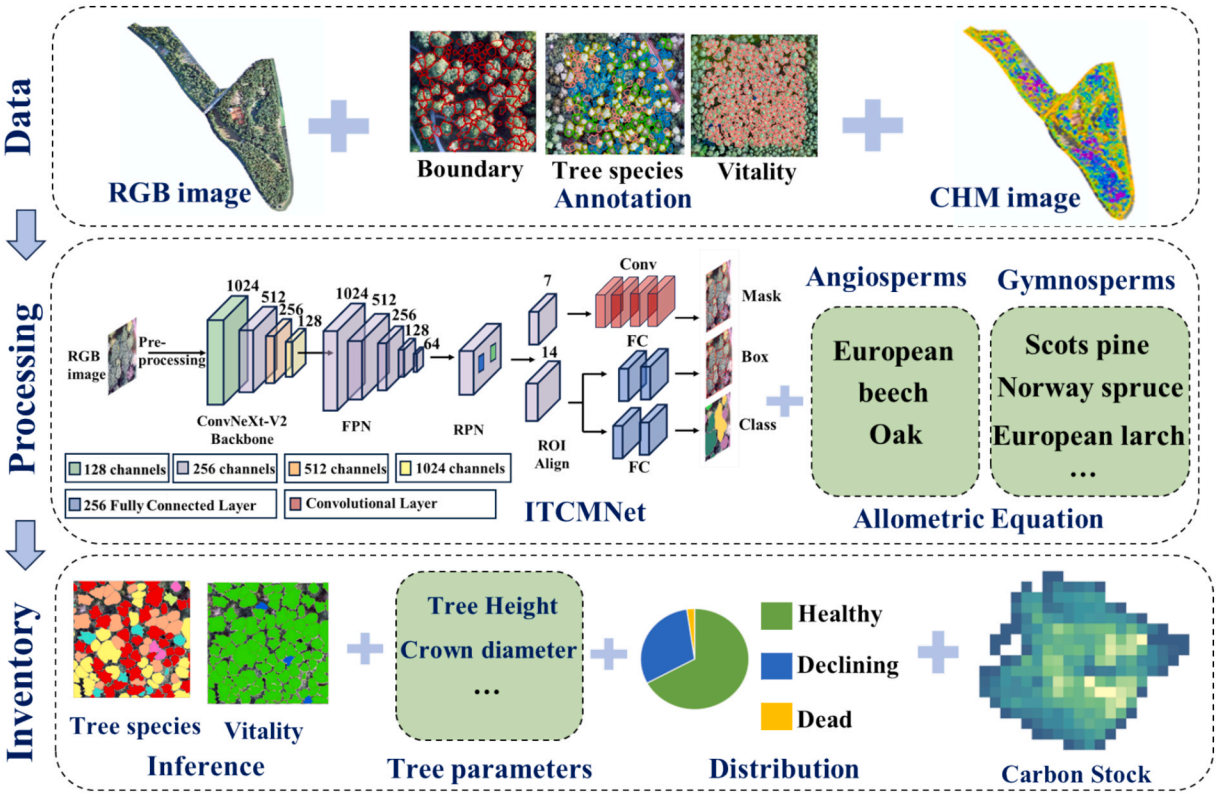

Fig. 2. The workflow of the proposed method.

2019) and trained on an Nvidia GeForce RTX 3080 GPU. The Bamberg dataset used consists of images with a resolution of 2048 × 2048 pixels, with 50% overlap in both horizontal and vertical directions. In the official BAMFORESTS benchmark, the data split of *Train-set, Test-set,* and *Val-set* is performed by plots rather than by tiles, ensuring that there is no overlap between plots across the different subsets. During ITCMNet training, Non-Maximum Suppression (NMS) is applied to the proposals generated by the RPN with an intersection over union (IoU) threshold of 0.4. This removes redundant candidate boxes before RCNN sampling. During inference, NMS is applied to the final RCNN-predicted BBox with an IoU threshold of 0.5, in order to minimize overlapping predictions. After completing the inference of segmentation and classification, the 2048 × 2048 sub-images are merged into full-forest images (Text S1; Supp Fig.A1). Two main challenges arise during this step. First, splitting the original image into sub-images may cause individual tree crowns to be divided at the edges. Second, due to overlap, the same tree crown may be detected multiple times in adjacent sub-images. To address these issues, a weighting rule based on the crown's distance and location is applied to identify and remove duplicate detections. Within each tile, overlapping polygons are analyzed by first removing any that are fully contained within another. If the overlap area exceeds 80%, the smaller polygon is deleted. For overlaps between 30% and 80%, the decision of which polygon to retain is made using a normalized composite score. This uses the combination of area and distance to the tile center through equal measuring. The complete model is constructed through three independent training processes and a final evaluation. One process is trained only on labeled data with canopy boundaries. Another process is trained on labeled data with canopy boundaries and labels for eight tree species. The remaining process uses a separate set of labeled data with canopy boundaries and labels for three tree vitality classes. A fixed framework with different strategies is applied across multiple subtasks to evaluate the model's performance in ITC segmentation, species classification, and vitality assessment, respectively. The proposed framework can predict all three tasks jointly or task-specific results. An increased number of categories generally leads to lower accuracy in the classification task. In order to mitigate the accuracy loss caused by excessive class numbers, the results of carbon stock estimation are based on the multi-task results of segmentation and tree species classification, as only these two outputs were required for the downstream carbon stock estimation.

3.2. Carbon stock estimation

High-quality individual tree delineation provides robust support for accurate estimation of morphological parameters. By integrating CHM with the results of individual tree delineation, three parameters were measured for the identified trees: tree height (T_H) and crown diameter (T_{cd}). CHM is calculated from difference between the DSM and DTM provided by the UAV data. Then, tree height is calculated by extracting the 95th percentile of maximum CHM values within the individual crown (De Petris et al., 2020). DSMs generated from UAV data may contain noise points that result in local extreme values. Such outliers can be avoided by using the 95th percentile of CHM maximum values (De Petris et al., 2020). Crown diameter is defined as the length of the longest side of the minimum BBox enclosing the tree crown.

$$T_{cd} = \max(CD_{NS}, CD_{WE}), \tag{1}$$

CD_{NS} is the north–south length of crown, CD_{WE} is the west-east length of crown.

Compared to labor-intensive field AGB measurements (e.g., cutting the whole trees), allometric model is the most popular method to estimate forest AGB over large geographical areas (de Tanago et al., 2018). In this study, the allometric equation is used to estimate AGB, which is difficult to measure directly, through a power-law relationship using tree attributes such as height and crown diameter that are easily measurable. Specifically, we employ the allometric model based on T_{cd} and T_H:

$$AGB = a^{*}(T_H{}^{*}T_{cd})^{b}, \quad (2)$$

where AGB is in unit kg/ha, and T_H and T_{cd} are in unit m. The parameter a is a dimensionless scale constant, while b is a dimensionless power exponent. Currently, there are no suitable allometric equations for local German products constructed as a function of tree height, crown diameter and AGB. In this study, there are two coefficients (a and b) that are determined from a global database including 2,395 trees that were cut and measured in great detail to quantify AGB, where a and b are 0.1113 and 1.79 for gymnosperm, and 0.0163 and 2.013 for angiosperm, respectively (Jucker et al., 2017). For trees classified as 'other', the allometric equation most closely related to that of angiosperms was applied. The majority of species within the 'Other' category are angiosperms, including Ulmus, Tilia, Sorbus Torminalis and Acer Pseudoplatanus. Due to their limited sample size, categorizing them as a distinct class is unlikely to bring significant practical benefits. Furthermore, previous studies have shown that the carbon fraction of AGB in forests is approximately 45% to 50% (Zhou et al., 2023). Internationally, the IPCC 2006 recommends using a conversion factor of 0.47 from AGB to carbon stock (Eggleston et al., 2006), which is a moderate value. Therefore, we assume that carbon stock (t/ha) accounts for 47% of their AGB in our study region (Eggleston et al., 2006; Santoro et al., 2021).

3.3. Evaluation

3.3.1. Assessment of ITC

Model performance for individual tree delineation is assessed using the mentioned BAMFORESTS benchmark data. Model evaluation is conducted at the tile level, and duplicate samples are removed. The performance of the models is evaluated by comparing the image annotations with the predictions of the algorithm using *precision*, *recall*, *F1 scores* and *IoU* as shown in the following equations. *Precision* is defined by calculating the number of correctly detected crowns as a proportion of the total number of crowns detected, and *recall* is defined by calculating the number of correctly detected crowns as a proportion of the total number of real crowns in the image. *Precision* and *recall* measure commission and omission errors in a result, respectively. The *F1 score* is the harmonic mean of *precision* and *recall*, evaluating the detection results' *precision* and completeness. *IoU* indicates the degree of overlap between the extracted crown boundaries and the ground truth.

For ITC tasks, the *IoU* between the annotation crown and the prediction crown is computed if the two are the only ones that correspond. In Table 3, B_{predict} indicates the predicted area of an individual tree, while B_{crown} delineates the extent of the annotated crown corresponding to this instance. If the IoU exceeds 0.5, it is defined as a true positive (TP). A false positive (FP) is defined as a predicted tree crown with an IoU less than 0.5 or a predicted tree crown that does not have the maximum IoU. If no prediction crown is found within the annotated crown, it is called a false negative (FN). Each predicted polygon is matched one-to-one with the ground truth tree crown that has the highest IoU. Once matched, the polygon is marked as used and excluded from subsequent matches.

Table 3
Experimental evaluation metrics.

	Metric	Formula
ITC Tasks	precision	$precision = \frac{TP}{TP+FP}$
	recall	$recall = \frac{TP}{TP+FN}$
	F1	$F1 = \frac{2{*}Precision{*}Recall}{Precision+Recall}$
	IoU	$IoU = \frac{area(B_{crown} \cap B_{predict})}{area(B_{crown} \cup B_{predict})}$
Carbon Stock	R^2	$R^2 = 1 - \frac{\sum_{i=1}^{n}(y_i - \widetilde{y_i})^2}{\sum_{i=1}^{n}(y_i - \overline{y_i})^2}$
	RMSE	$\text{RMSE} = \sqrt{\frac{1}{n-k-1}\sum_{i=1}^{n}(y_i - \widetilde{y_i})^2}$
	rRMSE	$\text{rRMSE} = \frac{RMSE}{\overline{y_i}}{*}100\%$
	bias	$\text{bias} = \frac{1}{n-1}\sum_{i=1}^{n}(y_i - \widetilde{y_i})$

3.3.2. Assessment of carbon stock

The accuracy of carbon stock estimation is assessed using plot-level data from *Test-set*, including four accuracy metrics, the coefficient of determination (R^2), root mean square error (RMSE), relative RMSE (rRMSE) and bias to evaluate the performance of the model. The R2 is used to quantify the proportion of variation in the dependent variable explained by the model's independent variables. The RMSE measures the model's prediction accuracy, with lower values indicating better performance. The rRMSE provides a measure of relative error. Bias represents the average difference between the predicted values and the actual values. The mentioned indicators are defined as shown in Table 3. Where n is the number of sample plots, k is the number of independent variables, y_i is the ground truth of the i th sample plot, $\widetilde{y_i}$ is the predicted value for the i^{th} sample plot, and $\overline{y}$ is the mean of the ground truth of the sample plots.

4. Results

4.1. Inference results of individual tree

4.1.1. Results of ITC delineation

The proposed deep learning framework ITCMNet effectively delineates tree boundaries and accurately identifies tree locations across varying forest types (Fig. 3). In the denser forests of Stadtwald and Tretzendorf area, as well as in the more fragmented landscape of the Hain region (with roads passing through), the algorithm consistently produces accurate segmentations that align closely with the annotated tree crowns. The model demonstrates robust segmentation capabilities across tree crowns of different sizes. Additionally, in the Tretzendorf area, where trees display varying levels of vitality, the algorithm successfully segments trees with different vitality statuses, such as healthy and dead trees. The proposed method is compared with two state-of-the-art ITC segmentation approaches, specifically YOLOEn (Straker et al., 2023) and a semi-supervised learning framework (SSL-MRCNN) (Wang et al., 2026), and the recent transformer framework Swin Transformer (Liu et al., 2022b). The YOLOEn is reported to achieve good performance across a wide range of forest types. The SSL-MRCNN has been extensively tested in three forest farms, yielding high accuracy (F1 $>$ 0.82). Specifically, we implemented SSL-MRCNN using its publicly available source code, while YOLOEn was reproduced based on the methodology described in its original publication. In order to ensure a fair comparison, all Swin Transformer, SSL-MRCNN and YOLOEn were configured with their default optimal hyperparameters, and all models were trained using the same number of epochs. As shown in Fig. 3, the YOLOEn method incorrectly extracted numerous shadow areas and performed over-segmentation, generating many small false tree crowns. Meanwhile, the SSL method produced significant omission errors for both dead and healthy trees. Compared with the Swin Transformer, the proposed method suffers from fewer over-segmentations in the Hain region. The qualitative results suggest that segmentation boundaries produced by the proposed method were precisely matched with ground truth annotations.

As for the quantitative evaluation shown in Table 4, ITCMNet achieved a higher precision (0.8) than the Swin Transformer (0.5), SSL-MRCNN (0.67), and YOLOEn (0.38), indicating that ITCMNet can effectively capture tree crown structures while minimizing false positives, thereby preventing the background from being misclassified as tree crowns and ensuring reliable segmentation results. Besides, the ITCMNet method achieves an obviously higher recall and F1 score

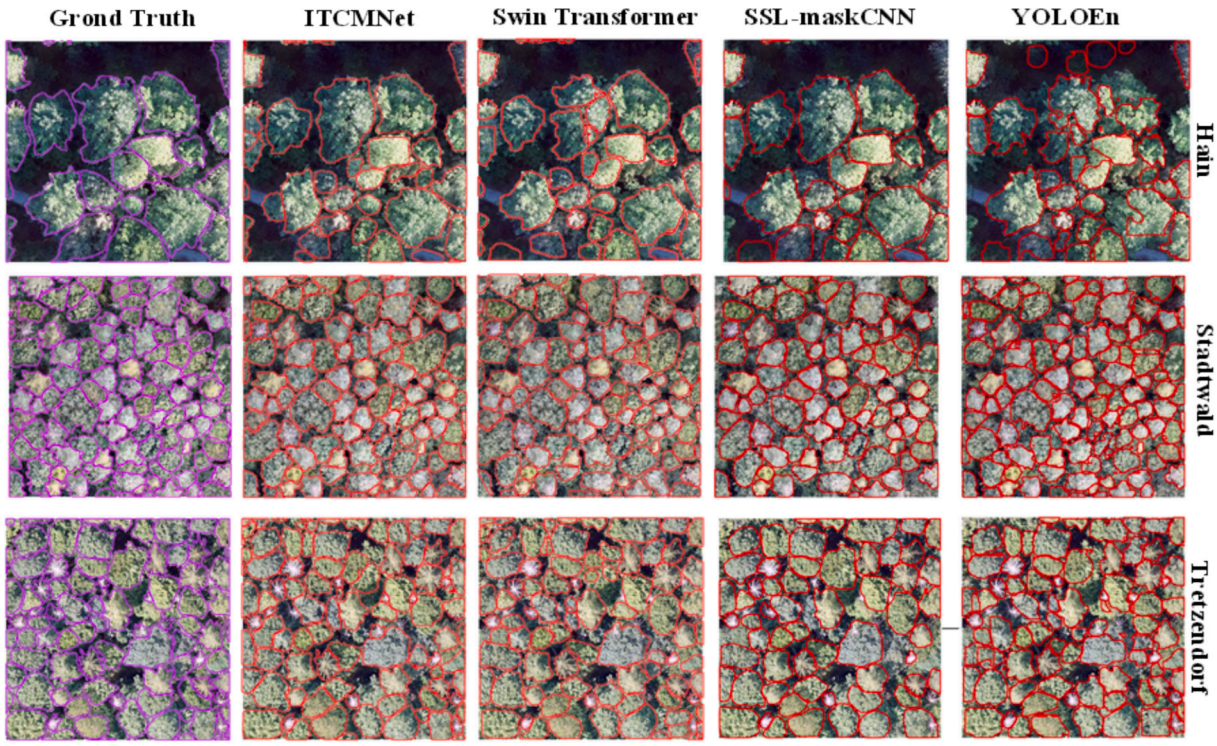

Fig. 3. Results comparison of ITCMNet to Swin Transformer (Liu et al., 2022a), SSL-maskCNN (Wang et al., 2026) and YOLOEn (Straker et al., 2023).

Table 4
Accuracy comparison of ITCMNet and three different methods.

Site		ITCMNet	Swin Transformer	SSL-MRCNN	YOLOEn
Hain	Precision	**0.67**	0.37	0.51	0.22
	Recall	**0.79**	0.52	0.5	0.31
	F1	**0.72**	0.43	0.51	0.26
Stadtwald	Precision	**0.91**	0.61	0.78	0.5
	Recall	**0.83**	0.68	0.69	0.57
	F1	**0.87**	0.64	0.73	0.53
Tretzendorf	Precision	**0.87**	0.62	0.75	0.48
	Recall	**0.81**	0.63	0.65	0.48
	F1	**0.84**	0.64	0.7	0.48
Total	Precision	**0.8**	0.51	0.67	0.38
	Recall	**0.81**	0.61	0.61	0.45
	F1	**0.81**	0.56	0.64	0.41

compared to other approaches in all three test regions. We have additionally compared the area distribution of four methods against the ground truth, as shown in Fig. 4. The frequency distribution of individual tree crowns reflects the occurrence of trees of varying sizes. If the model's distribution closely matches the ground truth, it indicates that the model not only predicts individual tree crowns accurately but also handles trees of various sizes robustly. We observed that the distribution generated by the ITCMNet method is closer to the ground-truth distribution of tree crowns, further supporting its effectiveness in accurately segmenting trees of different scales (Text S2; Table S1; Supp Fig. A2).

4.1.2. *Results of tree species classification*

U-Net is a widely adopted classification algorithm, frequently employed in the task of tree species classification (Schiefer et al., 2020; Weishaupt et al., 2025). In order to evaluate the efficacy of multi-task learning, a comparative analysis is conducted between U-Net and ITCMNet, the latter of which integrates instance segmentation with classification. As shown in Fig. 5, incorporating segmentation significantly improves classification performance. When using U-Net for pixel-wise classification, individual tree crowns are often erroneously segmented into multiple species due to a lack of neighborhood information constraints. In contrast, ITCMNet uses crown-level segmentation to extract spatially coherent features within each tree crown. This enables more accurate species discrimination and superior overall classification performance.

The proposed ITCMNet is then evaluated in the *Test-set*. The tree species classification results demonstrate good performance for common species, as shown in Table 5. Notably, *Norway spruce* achieves the highest *precision* of 0.92. For *Scots pine*, the algorithm also performs well, with a *precision* of 0.86. In contrast, for *European larch* we achieved an *F1* of 0.56, reflecting its more challenging classification. For the rarer species, *Douglas fir* and *silver fir*, both *accuracies* are low. This is primarily attributed to the small number of samples of these species, coupled with their spectral and morphological similarities to other gymnosperms, which makes them difficult to distinguish. Both species account for less than 1% of the total training samples, and the severe class imbalance contributes to the model's limited performance for these species.

Overall, the model achieves an average *F1 score* of 0.56, across all species, demonstrating acceptable performance for common tree species while encountering challenges in classifying rarer species. The inclusion of a large number of test plots containing previously unseen species resulted in the generation of numerous 'other' categories. Including such an '*other*' category is essential for practical applications. Especially for the classification of angiosperms and gymnosperms, the model achieved *F1 score* of 0.54 and 0.76, respectively, which is beneficial for the accurate estimation of carbon storage. Fig. 6 presents the inference results across the four regions, illustrating the area, proportion, and distribution of the tree species within the forest. The broader forest distribution is also assessed beyond the sample plot regions. The proportions of dominant species are approximately 50% in all four regions. In the Hain region, oak is the dominant species, covering 52.35%, while in Stadtwald, *Scots pine* is predominant, covering 48.90 ha and accounting for 51.11%. In the two Tretzendorf areas, *European beech* is dominant, covering 53.75% in Tretzendorf_1 and 46.56% in Tretzendorf_2. Except for Tretzendorf_2, which has the lowest proportion of *Douglas fir*, all other regions show a very low proportion of *silver fir*, occupying less than

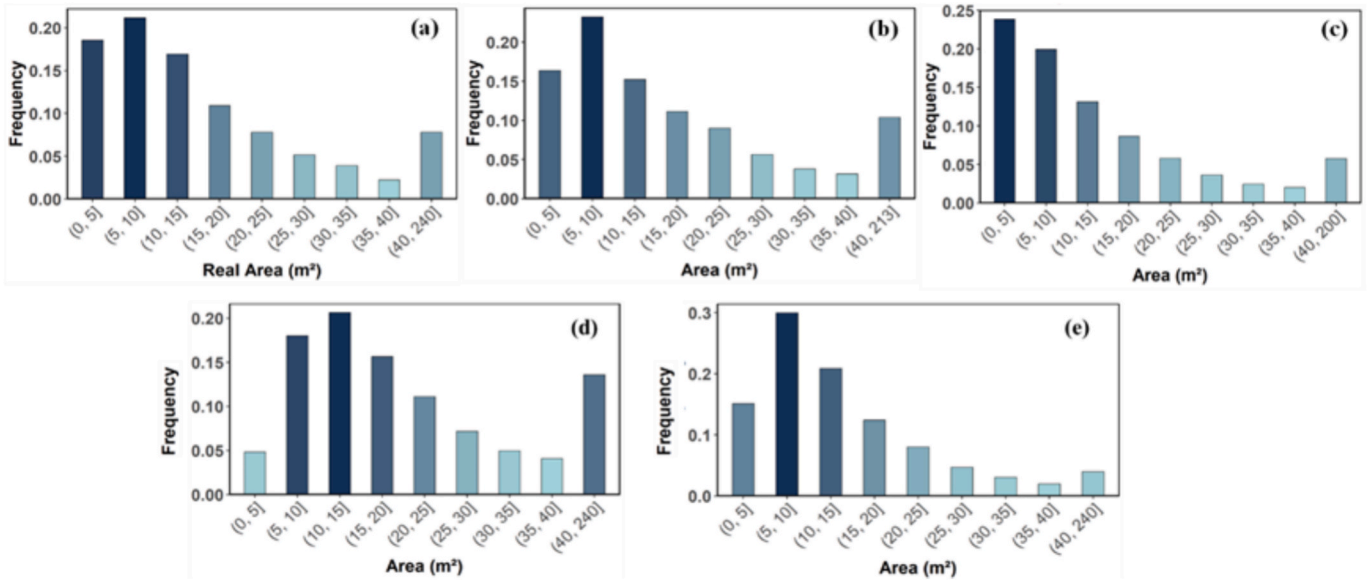

Fig. 4. Area distribution of individual tree crowns is presented by. (a) Ground Truth, (b) ITCMNet (c) Swin Transformer (d) SSL-MRCNN and (e) YOLOEn.

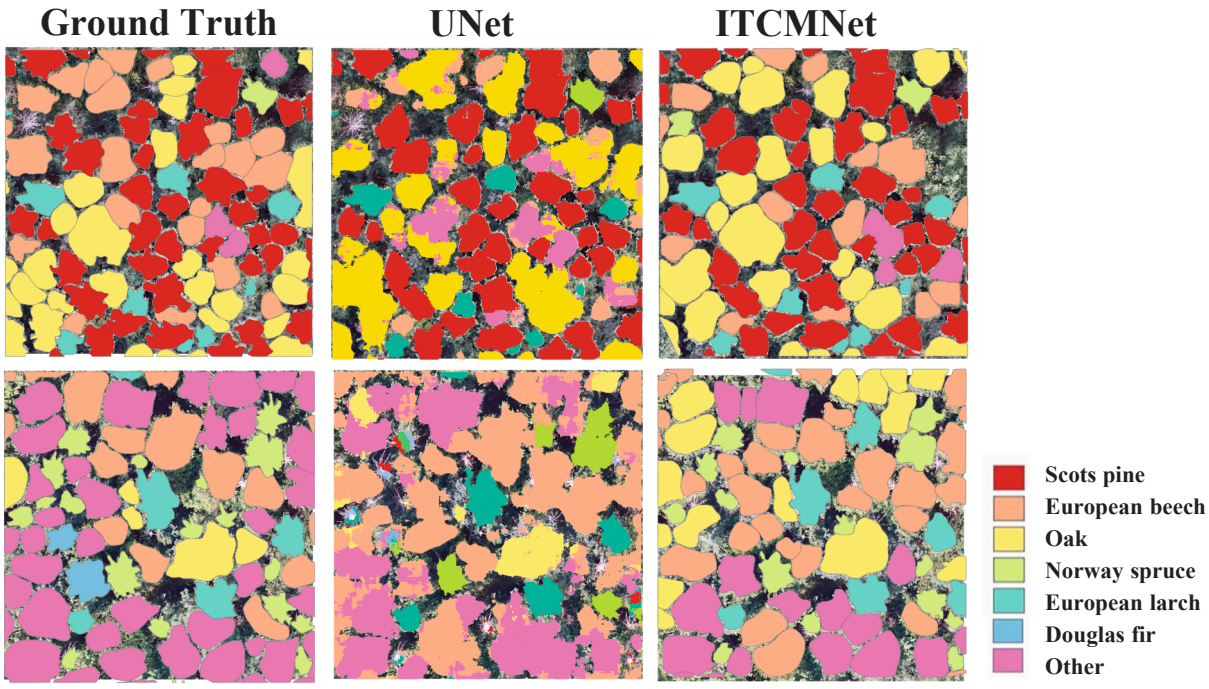

Fig. 5. Comparison of tree species classification results in detail.

Table 5
Accuracy of tree species classification at the individual tree level.

Spermatophyte	Tree species	TP	FP	FN	Precision	Recall	F1
angiosperms	European beech	2,750	2,986	2,112	0.48	0.57	0.52
	Oak	3,194	3,989	1,041	0.44	0.75	0.56
gymnosperms	Scots pine	2,895	470	686	0.86	0.81	0.83
	Norway spruce	674	61	529	0.92	0.56	0.7
	European larch	217	189	155	0.53	0.58	0.56
	Douglas fir	11	37	129	0.23	0.08	0.12
	Silver fir	0	0	112	0	0	0
Other	Other	1,185	1,049	3,858	0.53	0.24	0.33
Total	Total	10,926	8,781	8,622	0.55	0.56	0.56

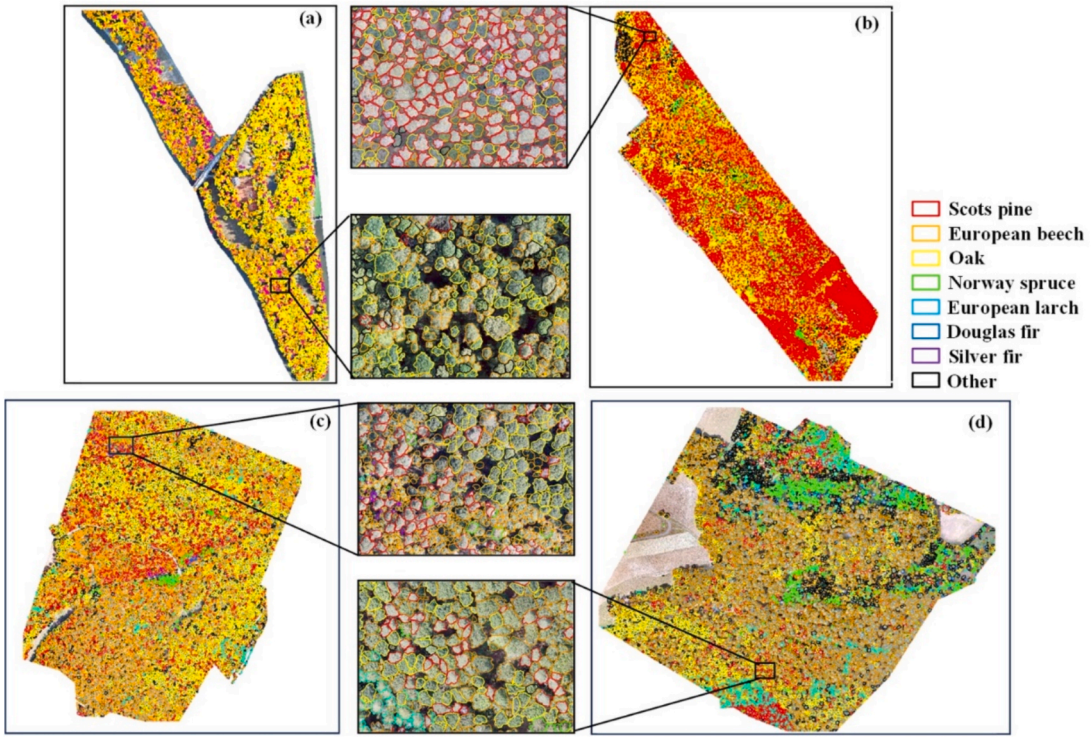

Fig. 6. Results of tree species classification at individual tree level. (a) Hain region, (b) Stadtwald region, (c) Tretzendorf_1 region, and (d) Tretzendorf_2 region.

0.02 ha. Significant differences are observed in the distribution patterns of tree species across regions. In Hain, *European beech* and *oak* are evenly distributed across the area. In contrast, *Scots pine* is concentrated along the borders of the region, while the central area is dominated by *European beech* and *oak*. In Tretzendorf_1, *Scots pine* and *oak* are primarily found in the northern part of the region, while *European beech* dominates the southern part. In Tretzendorf_2, *European beech* is widespread, with *Norway spruce* concentrated in the northern section and *Scots pine* primarily in the south.

4.1.3. Results of vitality estimation

As shown in Table 6, the ITCMNet method demonstrates the overall best performance in detecting healthy trees, achieving an F1 of 0.72. The detection *precision* for dead trees is 0.75, indicating that most dead trees are correctly classified. In comparison, distinguishing declining trees is more challenging, with an F1 score of 0.33, illustrating the difficulty in accurately identifying declining trees. Overall, the model achieves an F1 of 0.66. The model performs well in detecting dead trees and maintains a high precision for healthy trees, with further refinement needed to distinguish declining trees.

Fig. 7 illustrates the vitality, distribution area, and proportion of all trees across the four regions, extending beyond the plot areas. The proportion of healthy trees in all four areas is approximately 70%, except for the Stadtwald, which contains 2.31% dead trees, covering about 2.22 ha. The other three regions each have fewer than 1% dead trees. The distribution patterns further reveal that the Hain has the highest proportion of healthy trees, suggesting a more stable and thriving forest ecosystem. In contrast, a distinct area of tree mortality is evident in the center-left of the Stadtwald, indicating a potential need for timely human intervention to prevent further forest degradation. In Tretzendorf_1, declining trees are primarily concentrated in the central and southern parts of the region, while in Tretzendorf_2, declining trees are more evenly distributed across the entire area.

Table 6
Accuracy of vitality estimation at the individual tree level.

Vitality	TP	FP	FN	Precision	Recall	F1
Healthy	11,878	4,503	4,836	0.73	0.71	0.72
Decline	877	2,095	1,516	0.30	0.37	0.33
Dead	266	88	175	0.75	0.60	0.67
Total	13,021	6,686	6,527	0.66	0.67	0.66

4.2. Results of carbon stock estimation

Firstly, the height and crown diameter of individual trees are calculated. Subsequently, the AGB of individual trees is estimated based on tree parameters, species classification results and the allometric equations described above. The total AGB within each plot is then summed by tree region. Finally, the carbon stock of each plot is calculated using the carbon fraction coefficient. A total of 19,041 tree crowns from 29 sample plots of *Test-set* are included in the evaluation of the results. Compared to carbon stock estimation at the individual tree level, plot-level assessments help reduce errors caused by over-segmentation and provide a more accurate evaluation of model performance.

The calculated ground truth carbon stock from sample plot data is compared with the carbon stock inferred using the ITCMNet method. This method is evaluated by using the carbon stock assessment metrics, as shown in Fig. 8 and Table 7. The R^2 value of 0.83 indicates that the model achieves a good fit for estimating carbon stocks. The average difference between predicted and actual carbon stock is 7.94 Mg/ha and the value of rRMSE is 16.42%. The model maintains good predictive performance even in mixed forests with different tree species. A bias of −1.24 Mg/ha indicates a negative bias in the model, indicating a tendency to overestimate carbon stock by an average of 1.24 Mg/ha. This trend is further illustrated in the bias distribution shown in Fig. 8.

As shown in Table 7, the performance of the model in the *Test-set* is also compared by using the ESA CCI Biomass v5.0 satellite AGB product, German AGB products and Global Ecosystem Dynamics Investigation (GEDI) Level 4A (L4A) data (Dubayah et al., 2022; Kacic et al., 2023; Santoro and Cartus 2024). CCI Biomass v5.0 from 2021 is the latest available version, and GEDI L4A footprint data from the full year of 2022. Kriging interpolation is applied to convert the footprint-level AGB

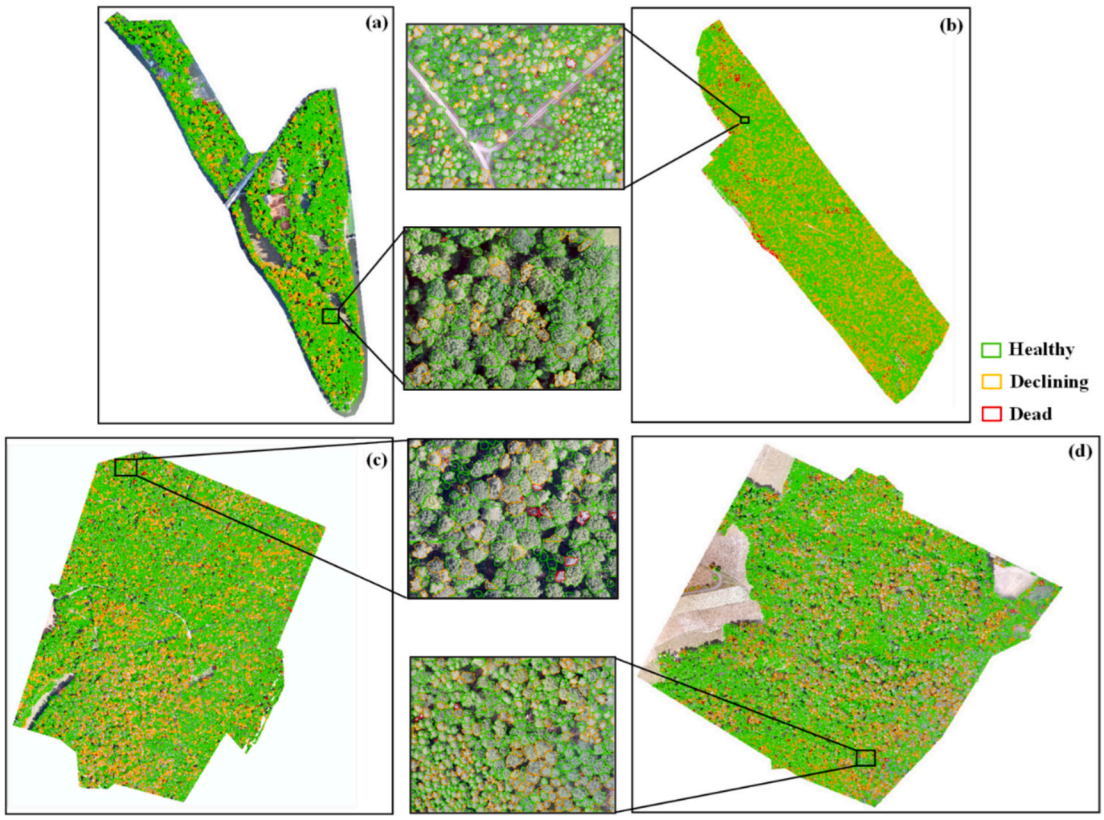

Fig. 7. Result of vitality estimation at individual tree level. (a) Hain region, (b) Stadtwald region, (c) Tretzendorf_1 region, and (d) Tretzendorf_2 region.

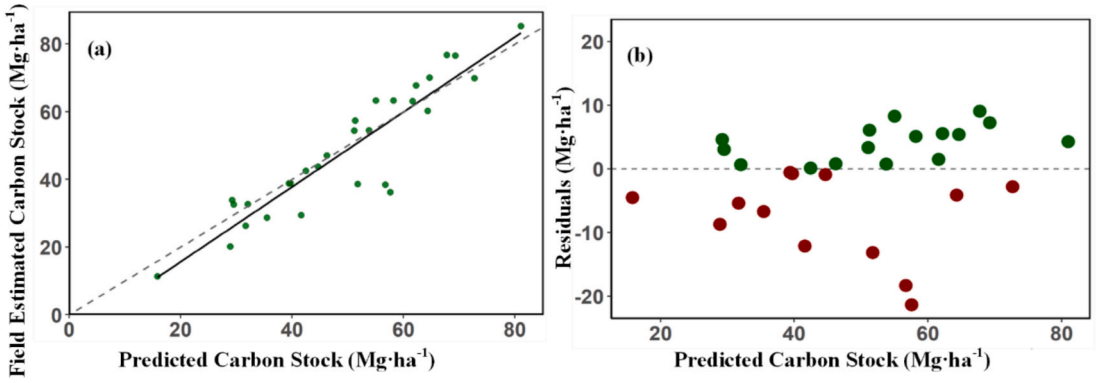

Fig. 8. Result of carbon stock estimation. (a) Scatterplots of predicted and estimated carbon stock, (b) Scatterplots of residuals and predicted carbon stock.

Table 7
Carbon stock estimation performance.

	R^2	RMSE (Mg/ha)	rRMSE	bias (Mg/ha)
This paper	0.83	7.94	16.42%	−1.24
CCI Biomass v5.0	−3.51	39.28	81.27%	−31.51
GEDI L4A	−1.23	27.62	57.16%	10.15
Kacic et al., (2023)	−9.93	48.38	128.83%	−49.00

values into a distribution map with a 100-meter resolution. AGB products for German forests are generated using GEDI data (Kacic et al., 2023). Our Test-set plots cover a total of 29 ha. However, this experiment is only conducted over the Stadtwald and Tretzendorf areas, due to null values of data for the Hain area in the mentioned German AGB product. Consequently, the evaluation is conducted using only the 14 ha of Stadtwald and Tretzendorf plots. Compared to the method proposed in this study, satellite-based products are more easily accessible and cost-effective, but their data accuracy in localized areas is lower. In contrast, the individual tree-level AGB product could generate outputs at various resolutions and demonstrates excellent model performance.

Based on UAV imagery from the four regions mentioned above, forest carbon storage distribution maps are generated at a coarser 1-hectare resolution for all AOIs, as shown in Fig. 9. Although carbon storage can be quantified at the individual tree level, coarser resolution carbon storage maps offer a broader perspective on regional carbon distribution and tree density patterns. Hain AOI is an urban forest park and the other three AOI are forests. Therefore, the other three AOI forests have a greater capacity for carbon sequestration. The edges of the AOI have only a small amount of tree distribution, so the carbon stock is relatively low.

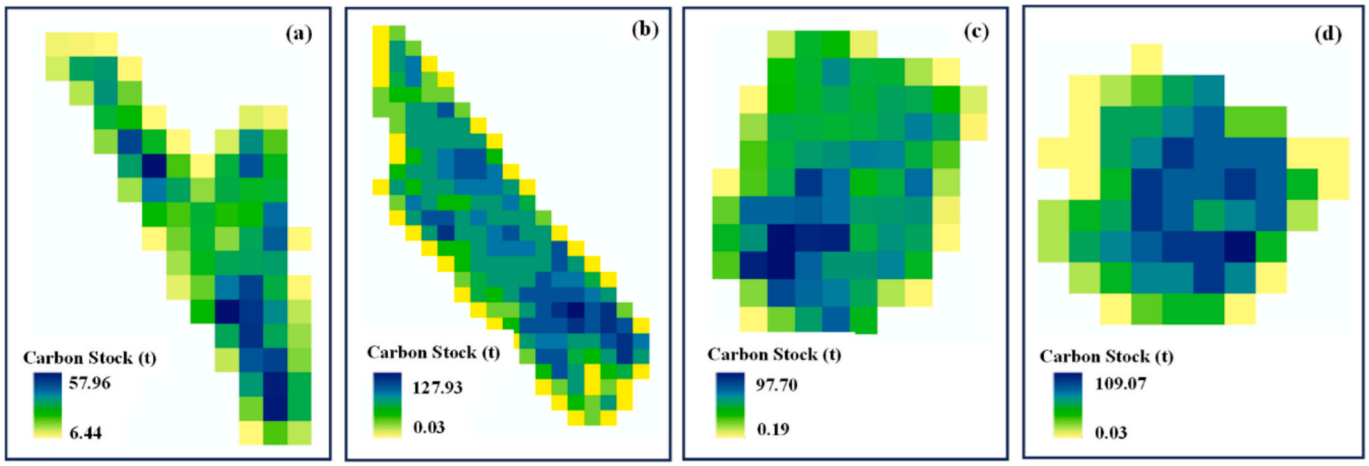

Fig. 9. Carbon stock estimation distribution. (a) Hain; (b) Stadtwald; (c) Tretzendorf_1; (d) Tretzendorf_2. (a, b, c, d) show estimations at 1-hectare resolution.

5. Discussion

5.1. Analysis of ITC

Forests provide biodiversity and ecosystem services. However, many disturbances to forests, including changes to their structure and function caused by factors such as hurricanes and pest outbreaks, occur at scales beyond the reach of direct field measurements. Therefore, utilizing remote sensing data to quantify changes of forest attributes is a critical issue in forest ecology and management (Weinstein et al., 2021b). Tree species classification is crucial for assessing ecosystem services and carbon storage (Zheng et al., 2021). Besides, tree vitality classification aids in estimating the health of forest ecosystems and carbon dynamics (Zuleta et al., 2023).

ITC delineation performance is influenced by many factors, such as forest type, leaf condition and RS data types (Yin and Wang 2016). In particular, coniferous forests differ from broadleaf forests in tree density and structure, leading to differences in model accuracy (Deluzet et al., 2022; Zhen et al., 2016). Although UAV imagery provides an ultra-high spatial resolution, segmenting dense, overlapping broadleaf crowns remain challenging and often results in over-segmentation or under-segmentation. The presence of fragmented crowns at subimage edges and differences in crown size across multiple species further increase the difficulty of model segmentation. Moreover, understory trees are even more difficult to detect beneath broadleaf trees. In contrast, coniferous forests generally have clearer crown boundaries, making segmentation easier (Xu et al., 2021).

Additionally, too few samples lead to the lack of transferability of the trained model (La Rosa et al., 2021). The study used datasets from multiple regions for training, testing and validation, meticulously annotating 27,160 samples. In this study, the method achieves an *F1* score of 0.72 for the Hain region, despite the lack of training data for these areas. This indicates that while the model successfully detects many tree crowns, a notable proportion of predictions are false positives. The recall is 0.79 in Hain region, suggesting that some tree crowns are still missed, possibly due to variations in tree species and crown sizes, which make it challenging for the model to fully capture all relevant features. The training data for this study were primarily collected in German forests. Recently, the first international contest ITD dataset from the International Society of Photogrammetry and Remote Sensing (ISPRS), which incorporates diverse forest types across eleven countries, offers superior global representativeness (Liang et al., 2026). As these contest data were not publicly available during this study's development phase, they were not included in the initial performance comparison. Future work will focus on evaluating and adapting the proposed approach across larger test regions.

In terms of tree species classification, compared to point-wise classification, ITCMNet integrates instance-level segmentation, incorporating more comprehensive information from ITC and resulting in improved classification performance (Yin and Wang 2016). Currently, the ITCMNet method relies solely on RGB imagery but still achieves relatively high accuracy in tree species classification without incorporating additional data sources. The performance of our approach is constrained by the following two issues. The first issue is sample imbalance. For instance, *Douglas fir* and *silver fir* account for less than 1% of the total training samples, resulting in a small sample size. This imbalance leads to reduced classification accuracy (Ren et al., 2020). The second issue is that our trained model is unable to encompass all unknown tree species, thus we have introduced an 'other' category. The 'other' category itself includes several minor species with tiny sample sizes, as well as when annotators are unable to accurately distinguish the exact tree species. In the BAMFORESTS dataset, the Hain forest is selected as a separate test dataset to have a certain domain gap to the train/val dataset. Misclassifications occurred because the species composition in the Hain region is neither consistent with that of the training area nor necessarily similar to the species in the 'other' category. In future data collection, we will place more emphasis on balancing the sample distribution among species to address the class imbalance issue, thereby improving classification accuracy and the robustness of model (Jackson and Adam 2021).

For vitality classification, the overall *precision* of the vitality classification for healthy and dead trees is around 0.75. However, the *precision* of detected declining trees is only 0.3, primarily because the UAV images contain only RGB bands. Changes in tree color are barely noticeable at the early stages of decline, making it difficult to accurately identify declining trees. To improve the accuracy of vitality classification, it is necessary to integrate multisource remote sensing data, such as hyperspectral imagery and LiDAR or phenological features extracted from time-series datasets. Combining these data sources would enhance the ability to capture spectral and structural differences among species and vitality levels (Abdollahnejad and Panagiotidis 2020; Qin et al., 2022). Hyperspectral imagery enables the retrieval of functional traits, such as chlorophyll and carotenoids, which reveal nutrient deficiencies and biotic stress caused by pests and diseases (Schneider et al., 2017). Meanwhile, LiDAR provides more three-dimensional tree structural information, enabling canopy density to be quantified (Acebes et al., 2021). The identification of tree species can be complicated by the complex structure of forests and environmental background, especially due to the similarity of spectral characteristics among different species. Therefore, incorporating seasonal variations in spectral signatures helps to improve tree classification (Su et al., 2025). Although this study has not further explored its potential for AGB and carbon stock estimation,

we plan to use vitality as a key data source in the future to optimize AGB modeling performance. In addition, we anticipate that this study will provide support for future forest management decisions, particularly in areas such as crop rotation, thinning and planting strategies, and contribute to long-term forest health monitoring with annual data (Li et al., 2021b).

5.2. Analysis of carbon stock estimation

Estimating carbon stocks is a core indicator for assessing the buffering capacity of forests against climate change. Compared to previous studies, the differences in AGB estimation in this paper are primarily due to variations in the data used. Firstly, AGB estimation is typically based on the diameter at breast height (DBH) method (Calders et al., 2015). The acquisition of DBH often requires point cloud data collected by LiDAR scanning systems, which is more expensive than UAV imagery (Fan et al., 2024). In contrast, this study primarily estimates AGB using allometric equations based on tree height and crown width, which are also highly reliable for both gymnosperms and angiosperms (Jucker et al., 2017). Secondly, although this study uses RGB imagery as a data source, the AGB modeling performance achieved is comparable to that of LiDAR data (Lu et al., 2020; Navarro et al., 2020). Despite the subpar segmentation and classification results, the estimation of carbon stocks shows sufficient performance. Broadleaf forests sometimes experience over-segmentation, which leads to an overestimation of AGB. Additionally, understory trees can be challenging to segment using only simple RGB bands (Latifi et al., 2015). Under-segmentation can result in an underestimation of AGB. Tree species classification is also crucial for biomass estimation, as it enables the application of different allometric models that better account for the varying relationships between tree parameters and biomass across tree species (Wu et al., 2025). The low classification accuracy of some tree species is due to the small number of samples and mis-segmentation, which has led to a certain degree of tree species misclassification. However, the major division of gymnosperms or angiosperms is not misclassified. Gymnosperms and angiosperms are already visually distinguished in imagery at a 1.6 cm resolution. Further investigations will be conducted to refine allometric equations, analyze variations among tree species, and assess the impact of health conditions on disparities in carbon sequestration among tree species.

Carbon storage in European mixed forests varies from tens to over a hundred tons per hectare (Avitabile et al., 2024). Specifically, the carbon stock in Germany ranges between 50 and 150 tons of carbon per hectare (t C/ha), which is consistent with our research findings. According to the 2012 National Forest Inventory (NFI) of Germany, (Wellbrock et al., 2017) estimated the aboveground carbon storage of beech forests to be 127t C/ha and that of spruce forests to be 101t C/ha. Plot-based surveys by (Förster et al., 2021) indicate that mature Scots pine forests have carbon stock of 86.8 ± 24.6 t C/ha, while young Scots pine forests average 72.0 ± 17.0t C/ha. Natural broadleaf forests display a higher average carbon stock of 147.2 ± 48.8t C/ha. Substantial variability in carbon storage is observed among different species, years and regions.

5.3. Potential of dense forest monitoring

Forest inventory could provide essential support for forest management in various aspects, such as timber yield estimation and natural disturbance monitoring, as illustrated in Fig. 10. This study uses UAV RGB imagery to explore tree attributes at the individual level. However, the parameters that can be provided by the sole imagery are limited. The DBH is measured using either point cloud data or field measurements, which are far more complex than processing imagery. Furthermore, integrating multiple data sources would present further method challenges. Although UAV imagery combined with deep learning cannot yet fully replace traditional forest inventories, it has been shown to be a cost-effective method of extracting individual tree parameters and has considerable potential for large-scale applications. Further investigation will be conducted to evaluate its effectiveness across additional datasets and regions for coarser resolution data sources. Although UAVs are limited to regional forest monitoring, they play a crucial role in bridging the gap between ground-based measurements and satellite observations. The spatial resolution of satellite remote sensors ranges from 1 m to 1 km, which cannot resolve spatial heterogeneity in a dense forest (Etteieb et al., 2013). In contrast, the abundant spatial context from ultra-high UAV images supports individual-tree level information detection, making it possible to scale from local forest inventory to regional forest investigation. Furthermore, the detailed regional forest information supports the further expansion to country-level forests or even global forests via satellite imagery (Chen et al., 2024; Lesiv et al., 2022). Therefore, the ITCMNet method demonstrates the great potential of portable UAVs to bridge the gap between forest inventory and satellite imagery for accurate and timely dense forest monitoring at a large scale.

6. Conclusion

This study proposes a comprehensive workflow for forest inventory and carbon storage estimation using UAV images. Deep learning combines ultra-high resolution remote sensing imagery and ground inventory data to enable automatic tree counting, species classification, vitality prediction, parameter estimation, and exploration of mixed forest resource surveys and tree distribution. Meanwhile, the model can achieve the estimation of forest carbon stock, which has the potential to be applied to large-scale dense forest carbon stock estimation and further improve the automation ability of forest resource monitoring. The results show that the mentioned workflow integrated with UAV data is portable for individual trees of different species. The ITC segmentation

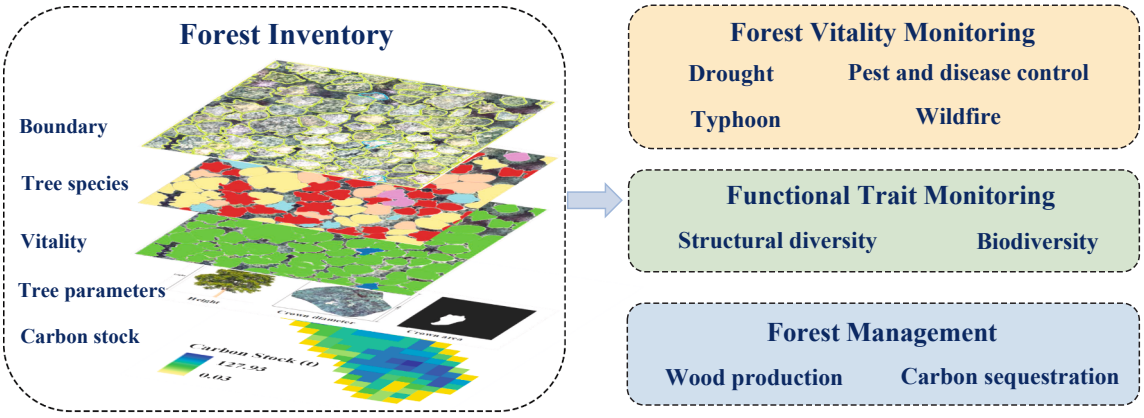

Fig. 10. Forest inventory data and applications.

achieved a recall of 0.81, a precision of 0.80, and an F1 score of 0.81. For tree species classification, the model achieved an accuracy of 0.54 for angiosperms and 0.76 for gymnosperms. Regarding the classification of tree vitality levels, the overall F1 reached 0.66 across the three defined vitality categories. For carbon stock estimation of mixed forest, the R^2 reached 0.83, with an rRMSE of 16.42%. Hence, the automation of forest health monitoring has improved. For different mixed forest areas, large-scale forest inventory and carbon stock assessment estimation at the individual tree level provide a sound data basis for forest applications to support further large-scale dense forest monitoring and management. On this basis, the research results have the potential to serve as an important reference for large-scale dense forest mapping, further enabling the effective integration of ground measurements and spatial surveying. Hence, applications such as spatio-temporal forest dynamic monitoring and carbon stock assessment can be multi-dimensionally supported.

Data availability

Inference results and code are available on the repository (https://github.com/WendyFan52/ITCMNet). The benchmark data have already been published (https://www.dlr.de/en/eoc/about-us/remote-sensing-technology-institute/photogrammetry-and-image-analysis/public-datasets/bamforests), and the tree species and vitality data are currently being prepared for publication. All the comparison experiment details and evaluation results were uploaded to GitHub and repository (https://github.com/QingWWWW/ITCS)(https://github.com/WendyFan52/yolov5) (https://zenodo.org/records/18485272).

Declaration of generative AI and AI-assisted technologies in the writing process

The authors used ChatGPT (GPT-4o, OpenAI) in order to check language and grammar errors. After using this tool, the authors reviewed and edited the content as needed and take full responsibility for the content of the publication.

CRediT authorship contribution statement

Wen Fan: Writing – original draft, Methodology, Formal analysis. **Thomas Knoke:** Writing – review & editing, Project administration. **Jonas Troles:** Resources, Data curation. **Jiaojiao Tian:** Writing – review & editing, Validation, Investigation.

Declaration of competing interest

The authors declare that they have no known competing financial interests or personal relationships that could have appeared to influence the work reported in this paper.

Acknowledgments

This research is supported by the China Scholarship Council and 3DforestSIF- Helmholtz Imaging Project (ZT-I-P-4-060). We thank Eleanor Gardner and Mareike Weishaupt for proofreading the manuscript.

Appendix A. Supplementary data

Supplementary data to this article can be found online at https://doi.org/10.1016/j.isprsjprs.2026.02.029.

References

Abdollahnejad, A., Panagiotidis, D., 2020. Tree species classification and health status assessment for a mixed broadleaf-conifer forest with UAS multispectral imaging. Remote Sens. 12, 3722.

Acebes, P., Lillo, P., Jaime-González, C., 2021. Disentangling LiDAR contribution in modelling species–habitat structure relationships in terrestrial ecosystems worldwide. a systematic review and future directions. Remote Sens. 13, 3447.

Agisoft, 2021. Metashape python reference. Release 1 (8), 4.

Avitabile, V., Pilli, R., Migliavacca, M., Duveiller, G., Camia, A., Blujdea, V., Adolt, R., Alberdi, I., Barreiro, S., Bender, S., et al., 2024. Harmonised statistics and maps of forest biomass and increment in Europe. Sci. Data 11, 274.

Brandt, M., Chave, J., Li, S., Fensholt, R., Ciais, P., Wigneron, J.-P., Gieseke, F., Saatchi, S., Tucker, C.J., Igel, C., 2024. High-resolution sensors and deep learning models for tree resource monitoring. Nat. Rev. Electr. Eng. 1–14.

Calders, K., Newnham, G., Burt, A., Murphy, S., Raumonen, P., Herold, M., Culvenor, D., Avitabile, V., Disney, M., Armston, J., et al., 2015. Nondestructive estimates of above-ground biomass using terrestrial laser scanning. Methods Ecol. Evol. 6, 198–208.

Chen, A., Xu, C., Zhang, M., Guo, J., Xing, X., Yang, D., Xu, B., Yang, X., 2024. Cross-scale mapping of above-ground biomass and shrub dominance by integrating UAV and satellite data in temperate grassland. Remote Sens. Environ. 304, 114024.

Chen, K., Wang, Jiaqi, Pang, J., Cao, Y., Xiong, Y., Li, X., Sun, S., Feng, W., Liu, Z., Xu, J., Zhang, Z., Cheng, D., Zhu, C., Cheng, T., Zhao, Q., Li, B., Lu, X., Zhu, R., Wu, Y., Dai, J., Wang, Jingdong, Shi, J., Ouyang, W., Loy, C.C., Lin, D., 2019. {MMDetection}: Open MMLab Detection Toolbox and Benchmark. arXiv Prepr. arXiv1906.07155.

De Petris, S., Berretti, R., Sarvia, F., Borgogno Mondino, E., 2020. When a definition makes the difference: Operative issues about tree height measures from RPAS-derived CHMs. iForest-Biogeosciences for. 13, 404.

de Tanago, J., Lau, A., Bartholomeus, H., Herold, M., Avitabile, V., Raumonen, P., Martius, C., Goodman, R.C., Disney, M., Manuri, S., et al., 2018. Estimation of above-ground biomass of large tropical trees with terrestrial LiDAR. Methods Ecol. Evol. 9, 223–234.

Deluzet, M., Erudel, T., Briottet, X., Sheeren, D., Fabre, S., 2022. Individual tree crown delineation method based on multi-criteria graph using geometric and spectral information: Application to several temperate forest sites. Remote Sens. 14, 1083.

Diez, Y., Kentsch, S., Fukuda, M., Caceres, M.L.L., Moritake, K., Cabezas, M., 2021. Deep learning in forestry using uav-acquired rgb data: A practical review. Remote Sens. 13, 2837.

Dubayah, R.O., Armston, J., Kellner, J.R., Duncanson, L., Healey, S.P., Patterson, P.L., Hancock, S., Tang, H., Bruening, J., Hofton, M.A., Blair, J.B., Luthcke, S.B., 2022. GEDI L4A footprint level aboveground biomass density. Version 2, 1. https://doi.org/10.3334/ORNLDAAC/2056.

Ecke, S., Stehr, F., Frey, J., Tiede, D., Dempewolf, J., Klemmt, H.-J., Endres, E., Seifert, T., 2024. Towards operational UAV-based forest health monitoring: Species identification and crown condition assessment by means of deep learning. Comput. Electron. Agric. 219, 108785.

Eggleston, H.S., Buendia, L., Miwa, K., Ngara, T., Tanabe, K., 2006. 2006 IPCC guidelines for national greenhouse gas inventories.

Etteieb, S., Louhaichi, M., Kalaitzidis, C., Gitas, I.Z., 2013. Mediterranean forest mapping using hyper-spectral satellite imagery. Arab. J. Geosci. 6, 5017–5032.

Fan, W., Tian, J., Knoke, T., Yang, B., Liang, F., Dong, Z., 2024. Investigating dual-source satellite image data and ALS data for estimating aboveground biomass. Remote Sens. 16, 1804.

Feng, Q., Liu, J., Gong, J., 2015. UAV remote sensing for urban vegetation mapping using random forest and texture analysis. Remote Sens. 7, 1074–1094.

Ferrara, C., Chianucci, F., Bajocco, S., 2023. On the temporal mismatch between in-situ and satellite-derived spring phenology of European beech forests. Int. J. Remote Sens. 44, 1684–1701.

Förster, A., Culmsee, H., Leuschner, C., 2021. Thinned northern German Scots pine forests have a low carbon storage and uptake potential in comparison to naturally developing beech forests. For. Ecol. Manage. 479, 118575.

Hahn, W.A., Knoke, T., 2010. Sustainable development and sustainable forestry: analogies, differences, and the role of flexibility. Eur. J. For. Res. 129, 787–801.

Hartling, S., Sagan, V., Maimaitijiang, M., 2021. Urban tree species classification using UAV-based multi-sensor data fusion and machine learning. Giscience Remote Sens. 58, 1250–1275.

He, K., Gkioxari, G., Dollár, P., Girshick, R., 2017. Mask r-cnn, in. In: Proceedings of the IEEE International Conference on Computer Vision, pp. 2961–2969.

Hu, T., Sun, X., Su, Y., Guan, H., Sun, Q., Kelly, M., Guo, Q., 2020. Development and performance evaluation of a very low-cost UAV-LiDAR system for forestry applications. Remote Sens. 13, 77.

Jackson, C.M., Adam, E., 2021. Machine learning classification of endangered tree species in a tropical submontane forest using worldview-2 multispectral satellite imagery and imbalanced dataset. Remote Sens. 13, 4970.

Jing, L., Hu, B., Noland, T., Li, J., 2012. An individual tree crown delineation method based on multi-scale segmentation of imagery. ISPRS J. Photogramm. Remote Sens. 70, 88–98.

Jucker, T., Caspersen, J., Chave, J., Antin, C., Barbier, N., Bongers, F., Dalponte, M., van Ewijk, K.Y., Forrester, D.I., Haeni, M., et al., 2017. Allometric equations for integrating remote sensing imagery into forest monitoring programmes. Glob. Chang. Biol. 23, 177–190.

Kacic, P., Thonfeld, F., Gessner, U., Kuenzer, C., 2023. Forest structure characterization in Germany: novel products and analysis based on GEDI, Sentinel-1 and Sentinel-2 data. Remote Sens. 15, 1969.

Kempf, C., Tian, J., Kurz, F., D'Angelo, P., Schneider, T., Reinartz, P., 2021. Oblique view individual tree crown delineation. Int. J. Appl. Earth Obs. Geoinf. 99, 102314.

Knoke, T., Hanley, N., Roman-Cuesta, R.M., Groom, B., Venmans, F., Paul, C., 2023. Trends in tropical forest loss and the social value of emission reductions. Nat. Sustain. 6, 1373–1384.

Knutzen, F., Averbeck, P., Barrasso, C., Bouwer, L.M., Gardiner, B., Grünzweig, J.M., Hänel, S., Haustein, K., Johannessen, M.R., Kollet, S., et al., 2025. Impacts on and damage to European forests from the 2018–2022 heat and drought events. Nat. Hazards Earth Syst. Sci. 25, 77–117.

La Rosa, L.E.C., Sothe, C., Feitosa, R.Q., de Almeida, C.M., Schimalski, M.B., Oliveira, D. A.B., 2021. Multi-task fully convolutional network for tree species mapping in dense forests using small training hyperspectral data. ISPRS J. Photogramm. Remote Sens. 179, 35–49.

Latifi, H., Fassnacht, F.E., Müller, J., Tharani, A., Dech, S., Heurich, M., 2015. Forest inventories by LiDAR data: A comparison of single tree segmentation and metric-based methods for inventories of a heterogeneous temperate forest. Int. J. Appl. Earth Obs. Geoinf. 42, 162–174.

Lechner, A.M., Foody, G.M., Boyd, D.S., 2020. Applications in remote sensing to forest ecology and management. One Earth 2, 405–412.

Lesiv, M., Schepaschenko, D., Buchhorn, M., See, L., Dürauer, M., Georgieva, I., Jung, M., Hofhansl, F., Schulze, K., Bilous, A., et al., 2022. Global forest management data for 2015 at a 100 m resolution. Sci. Data 9, 199.

Li, S., Brandt, M., Fensholt, R., Kariryaa, A., Igel, C., Gieseke, F., Nord-Larsen, T., Oehmcke, S., Carlsen, A.H., Junttila, S., et al., 2023. Deep learning enables image-based tree counting, crown segmentation, and height prediction at national scale. PNAS Nexus 2, pgad076.

Li, Y., He, J., Lu, L., Xu, J., Wang, H., Ye, S., 2021a. The long-term effects of thinning and mixing on species and structural diversity of Chinese fir plantations. New For. 52, 285–302.

Li, Z., Liu, F., Yang, W., Peng, S., Zhou, J., 2021b. A survey of convolutional neural networks: analysis, applications, and prospects. IEEE Trans. Neural Networks Learn. Syst. 33, 6999–7019.

Liang, X., Chen, J., Gong, W., Puttonen, E., Wang, Y., 2025. Influence of data and methods on high-resolution imagery-based tree species recognition considering phenology: The case of temperate forests. Remote Sens. Environ. 323, 114654.

Liang, X., Kukko, A., Balenović, I., Saarinen, N., Junttila, S., Kankare, V., Holopainen, M., Mokroš, M., Surov\'y, Kaartinen, P.H., 2022. Others, close-range remote sensing of forests: The state of the art, challenges, and opportunities for systems and data acquisitions. IEEE Geosci. Remote Sens. Mag. 10, 32–71.

Liang, X., Wang, Y., Pan, J., Heiskanen, J., Wang, N., Wu, S., Vuorinne, I., Tian, J., Troles, J., Cloutier, M., et al., 2026. Empowering tree-scale monitoring over large areas: Individual tree delineation from high-resolution imagery. ISPRS J. Photogramm. Remote Sens. 232, 974–999.

Lin, T.-Y., Maire, M., Belongie, S., Hays, J., Perona, P., Ramanan, D., Dollár, P., Zitnick, C.L., 2014. Microsoft coco: Common objects in context, in: Computer Vision–ECCV 2014: 13th European Conference, Zurich, Switzerland, September 6-12, 2014, Proceedings, Part v 13. pp. 740–755.

Liu, Y., Chen, D., Fu, S., Mathiopoulos, P.T., Sui, M., Na, J., Peethambaran, J., 2024. Segmentation of individual tree points by combining marker-controlled watershed segmentation and spectral clustering optimization. Remote Sens. 16, 610.

Liu, Z.e., Hu, H., Lin, Y., Yao, Z., Xie, Z., Wei, Y., Ning, J., Cao, Y., Zhang, Z., Dong, L., et al., 2022a. Swin transformer v2: Scaling up capacity and resolution. In: In: Proceedings of the IEEE/CVF Conference on Computer Vision and Pattern Recognition, pp. 12009–12019.

Liu, Z., Mao, H., Wu, C.-Y., Feichtenhofer, C., Darrell, T., Xie, S., 2022b. A convnet for the 2020s. In: In: Proceedings of the IEEE/CVF Conference on Computer Vision and Pattern Recognition, pp. 11976–11986.

Lu, J., Wang, H., Qin, S., Cao, L., Pu, R., Li, G., Sun, J., 2020. Estimation of aboveground biomass of Robinia pseudoacacia forest in the yellow river delta based on UAV and backpack LiDAR point clouds. Int. J. Appl. Earth Obs. Geoinf. 86, 102014.

Navarro, A., Young, M., Allan, B., Carnell, P., Macreadie, P., Ierodiaconou, D., 2020. The application of Unmanned Aerial Vehicles (UAVs) to estimate above-ground biomass of mangrove ecosystems. Remote Sens. Environ. 242, 111747.

Nevalainen, O., Koivumäki, N., Oliveira, R.A., Hakala, T., Näsi, R., Liang, X., Wang, Y., Hyyppä, J., Honkavaara, E., 2025. Drone imaging-based wall-to-wall processing pipelines for individual tree level inventory in boreal forest plots. ISPRS Open J. Photogramm, Remote Sens.

Puliti, S., Ene, L.T., Gobakken, T., Næsset, E., 2017. Use of partial-coverage UAV data in sampling for large scale forest inventories. Remote Sens. Environ. 194, 115–126.

Qin, H., Zhou, W., Yao, Y., Wang, W., 2022. Individual tree segmentation and tree species classification in subtropical broadleaf forests using UAV-based LiDAR, hyperspectral, and ultrahigh-resolution RGB data. Remote Sens. Environ. 280, 113143.

Ren, Y., Zhang, X., Ma, Y., Yang, Q., Wang, C., Liu, H., Qi, Q., 2020. Full convolutional neural network based on multi-scale feature fusion for the class imbalance remote sensing image classification. Remote Sens. 12, 3547.

Riedel, T., Bender, S., Hennig, P., Kroiher, F., Schnell, S., Schwitzgebel, F., Stauber, T., Stahlmann, J.K., Kühling, M., 2024. Der Wald in Deutschland. Ausgewählte Ergebnisse der vierten Bundeswaldinventur.

Santoro, M., Cartus, O., 2024. ESA Biomass Climate Change Initiative (Biomass_cci): Global datasets of forest above-ground biomass for the years 2010, 2015, 2016, 2017, 2018, 2019, 2020 and 2021, v5. https://doi.org/10.5285/02e1b18071ad45a19b4d3e8adafa2817.

Santoro, M., Cartus, O., Carvalhais, N., Rozendaal, D.M.A., Avitabile, V., Araza, A., De Bruin, S., Herold, M., Quegan, S., Rodr\'\iguez-Veiga, P., 2021. Others, The global forest above-ground biomass pool for 2010 estimated from high-resolution satellite observations. Earth Syst. Sci. Data 13, 3927–3950.

Schiefer, F., Kattenborn, T., Frick, A., Frey, J., Schall, P., Koch, B., Schmidtlein, S., 2020. Mapping forest tree species in high resolution UAV-based RGB-imagery by means of convolutional neural networks. ISPRS J. Photogramm. Remote Sens. 170, 205–215.

Schneider, F.D., Morsdorf, F., Schmid, B., Petchey, O.L., Hueni, A., Schimel, D.S., Schaepman, M.E., 2017. Mapping functional diversity from remotely sensed morphological and physiological forest traits. Nat. Commun. 8, 1441.

Straker, A., Puliti, S., Breidenbach, J., Kleinn, C., Pearse, G., Astrup, R., Magdon, P., 2023. Instance segmentation of individual tree crowns with YOLOv5: A comparison of approaches using the ForInstance benchmark LiDAR dataset. ISPRS Open J. Photogramm. Remote Sens. 9, 100045.

Su, Y., Li, J., Smith, A.R., Yan, X., Ma, T., Zhang, J., Chen, D., 2025. Identification of tree species using machine learning and phenological characteristics from a 4-year time series of remote sensing data. Int. J. Remote Sens. 46, 6377–6402.

Tochon, G., Féret, J.-B., Valero, S., Martin, R.E., Knapp, D.E., Salembier, P., Chanussot, J., Asner, G.P., 2015. On the use of binary partition trees for the tree crown segmentation of tropical rainforest hyperspectral images. Remote Sens. Environ. 159, 318–331.

Troles, J., Schmid, U., Fan, W., Tian, J., 2024. BAMFORESTS: Bamberg benchmark forest dataset of individual tree crowns in very-high-resolution UAV images. Remote Sens. 16, 1935.

Vermessungsverwaltung, B., 2022. DGM1 — Bayerische Geodaten (Open Data).

Wagner, F.H., Ferreira, M.P., Sanchez, A., Hirye, M.C.M., Zortea, M., Gloor, E., Phillips, O.L., de Souza Filho, C.R., Shimabukuro, Y.E., Aragão, L.E.O.C., 2018. Individual tree crown delineation in a highly diverse tropical forest using very high resolution satellite images. ISPRS J. Photogramm. Remote Sens. 145, 362–377.

Wallace, L., Lucieer, A., Watson, C., Turner, D., 2012. Development of a UAV-LiDAR system with application to forest inventory. Remote Sens. 4, 1519–1543.

Wang, Q., Zhao, Y., Che, Y., Shen, H., Qiu, Y., Wang, Y., 2026. A semi-supervised framework for UAV-based individual tree crown segmentation in structurally heterogeneous planted forests. Int. J. Appl. Earth Obs. Geoinf. 146, 105078.

Weinstein, B.G., Graves, S.J., Marconi, S., Singh, A., Zare, A., Stewart, D., Bohlman, S.A., White, E.P., 2021a. A benchmark dataset for canopy crown detection and delineation in co-registered airborne RGB, LiDAR and hyperspectral imagery from the national ecological observation network. PLoS Comput. Biol. 17, e1009180.

Weinstein, B.G., Marconi, S., Bohlman, S.A., Zare, A., Singh, A., Graves, S.J., White, E.P., 2021b. A remote sensing derived data set of 100 million individual tree crowns for the national ecological observatory network. Elife 10, e62922.

Weishaupt, M., Fan, W., Troles, J., Tian, J., 2025. Individual Tree Crown Based Tree Species Classification from Very High-Resolution UAV Images.

Wellbrock, N., Grüneberg, E., Riedel, T., Polley, H., 2017. Carbon stocks in tree biomass and soils of German forests. Cent. Eur. for. J. 63, 105.

Wen, F., Tian, J., Troles, J., Döllerer, M., Kindu, M., Knoke, T., 2024. Comparing deep learning and MCWST approaches for individual tree crown segmentation. Int. Soc. Photo. Remote Sens. 1–7.

Woo, S., Debnath, S., Hu, R., Chen, X., Liu, Z., Kweon, I.S., Xie, S., 2023. Convnext v2: Co-designing and scaling convnets with masked autoencoders. In: In: Proceedings of the IEEE/CVF Conference on Computer Vision and Pattern Recognition, pp. 16133–16142.

Wu, Z., Liu, X., Cheng, S., Yang, C., Wang, Z., Liu, Y., Dong, L., Li, F., Hao, Y., 2025. Evaluating the effectiveness of forest type stratification for aboveground biomass inference. Int. J. Appl. Earth Obs. Geoinf. 143, 104829.

Xu, W., Deng, S., Liang, D., Cheng, X., 2021. A crown morphology-based approach to individual tree detection in subtropical mixed broadleaf urban forests using UAV LiDAR data. Remote Sens. 13, 1278.

Yao, L., Liu, T., Qin, J., Lu, N., Zhou, C., 2021. Tree counting with high spatial-resolution satellite imagery based on deep neural networks. Ecol. Ind. 125, 107591.

Yin, D., Wang, L., 2016. How to assess the accuracy of the individual tree-based forest inventory derived from remotely sensed data: A review. Int. J. Remote Sens. 37, 4521–4553.

Zhen, Z., Quackenbush, L.J., Zhang, L., 2016. Trends in automatic individual tree crown detection and delineation—Evolution of LiDAR data. Remote Sens. 8, 333.

Zheng, J., Fu, H., Li, W., Wu, W., Yu, L., Yuan, S., Tao, W.Y.W., Pang, T.K., Kanniah, K.D., 2021. Growing status observation for oil palm trees using unmanned aerial vehicle (UAV) images. ISPRS J. Photogramm. Remote Sens. 173, 95–121.

Zhou, X., Hu, C., Wang, Z., 2023. Distribution of biomass and carbon content in estimation of carbon density for typical forests. Glob. Ecol. Conserv. 48, e02707.

Zuleta, D., Arellano, G., McMahon, S.M., Aguilar, S., Bunyavejchewin, S., Castaño, N., Chang-Yang, C.-H., Duque, A., Mitre, D., Nasardin, M., et al., 2023. Damage to living trees contributes to almost half of the biomass losses in tropical forests. Glob. Chang. Biol. 29, 3409–3420.